Systemic dissemination, reproductive tissue tropism and gestational stage-dependent placental responses during Mayaro virus infection in a murine model

Arévalo A.P.[1], Perbolianachis P.[2,3], Pórfido J.L.[1], Pereira-Gómez M.[2,4], Greif G.[5], Hurtado J.[2,3], Fajardo A.[2,3], Varela B.[6], Verdes J.M.[6], Moratorio G.[2,3*], Crispo M[1*].

[1] Laboratory Animal Biotechnology Unit, Institut Pasteur de Montevideo, Uruguay

[2] Experimental Virus Evolution Laboratory, Institut Pasteur de Montevideo, Uruguay

[3] Laboratory of Molecular Virology, Nuclear Research Center, Faculty of Sciences, Udelar

[4] Microbiology Unit, Department of Pathobiology, Faculty of Veterinary Medicine, Udelar

[5] Laboratorio de Interacción Hospedero-Patógeno, Institut Pasteur de Montevideo, Uruguay

[6] Pathology Unit, Department of Pathobiology, Faculty of Veterinary Medicine, Udelar

[*] Corresponding authors: crispo@pasteur.edu.uy; moratorio@pasteur.edu.uy

Abstract

Mayaro virus (MAYV) is an emerging mosquito-borne alphavirus associated with acute febrile illness and persistent arthralgia, with increasing reports in Latin America and potential for geographic expansion. However, its dissemination dynamics, tissue tropism and transmission routes remain incompletely defined. Here, we developed a murine model to characterize systemic viral dissemination, tissue tropism and the impact of gestational stage on maternal–fetal outcomes. A nanoluciferase-expressing MAYV reporter enabled non-invasive *in vivo* imaging, revealing rapid and widespread systemic dissemination under controlled conditions. Complementary infection with wild-type (WT) virus confirmed broad tropism across lymphoid, musculoskeletal and reproductive tissues. At 24 hours post-infection (hpi), viral distribution was relatively homogeneous across tissues, whereas at 48 hpi, tissue-specific differences emerged, with increased viral loads in selected organs, including the spleen and male reproductive tissues. Transient sex-dependent differences were observed at 24 hpi but were not sustained at later time points. Hematological and biochemical analyses revealed early systemic alterations consistent with changes in leukocyte distribution during acute infection. Infectious viral particles were detected in reproductive tissues of both sexes, including in sperm, supporting the biological plausibility of non-vector transmission, although detection in exposed animals was limited. Gestational stage influenced infection outcomes: early gestation (infected at 7.5–8.5 dpc; analyzed at 9.5–10.5 dpc) was associated with detection of infectious virus in fetal tissues, whereas mid-gestation (infected at 13.5–14.5 dpc; analyzed at 15.5–16.5 dpc) showed no detectable infectious virus in fetuses despite evidence of viral antigen persistence and sustained infectious viral presence in maternal and placental compartments. Together, these findings provide a preclinical framework

for investigating MAYV pathogenesis and underscore the role of tissue tropism and gestational context in shaping infection dynamics and maternal–fetal involvement.

KEYWORDS: Mayaro virus; viral pathogenesis; Emerging arbovirus; Vertical transmission; Systemic dissemination; Placental infection; Murine model; *in vivo* imaging

Author summary

Mayaro virus (MAYV) is an emerging mosquito-borne virus that causes fever and long-lasting joint pain, with increasing reports in Latin America and potential for wider geographic spread. Despite its growing relevance, key aspects of MAYV pathogenesis remain to be fully defined, including the mechanisms underlying systemic dissemination and tissue tropism, as well as its potential to affect pregnancy or be transmitted through non-vector routes. Here, we used a mouse model with a luminescent reporter virus to track MAYV dissemination *in vivo*, revealing rapid and widespread distribution across multiple tissues. In studies using wild-type virus, infectious virus was detected not only in muscle and immune-related organs but also in reproductive tissues of both females and males. Importantly, gestational stage influenced viral distribution. When infection occurred early in gestation, infectious viral particles were detected in fetal tissues. In contrast, at later stages of pregnancy, infectious virus was no longer detectable in fetuses, despite evidence of viral antigen persistence and sustained infectious viral presence in maternal and placental tissues. Together, these findings advance our understanding of MAYV infection, highlight gestational timing as a factor associated with fetal exposure and suggest the possibility of transmission through routes other than mosquitoes, providing a framework for future studies on this emerging virus.

Introduction

Mayaro virus (MAYV), an emerging arbovirus of the *Alphavirus* genus and *Togaviridae* family, was first identified in Trinidad and Tobago in 1954 and has since been responsible for sporadic outbreaks across Central and South America. Imported cases have also been reported in Europe and North America, raising concerns at the international public health level as reflected in the epidemiological alert issued by the Pan American Health Organization / World Health Organization in May 2019, which emphasized the need to strengthen epidemiological surveillance and laboratory diagnostic capacity (1). The virus has already been detected in Brazil, Peru, Venezuela, Suriname, Colombia, Ecuador, Bolivia and Panama, with serological evidence also reported in Costa Rica, Guatemala, Mexico and Haiti (2-5). Multiple anthropogenic factors—including climate change, urbanization, human mobility and the expanding distribution of mosquito vectors such as *Aedes aegypti* and *Aedes albopictus*—contribute to the increasing risk of MAYV geographic expansion, even in countries without active transmission. A recent study estimated that 58.9 million people in Latin America reside in ecologically suitable areas for MAYV transmission (6, 7). From a genomic perspective, MAYV possesses a positive-sense single-stranded RNA genome of approximately 11.5 kb, which encodes both non-structural (nsP1–nsP4) and structural proteins (CP, E3, E2, TF, 6k and E1) through two open reading frames (ORFs). The virion is enveloped in a lipid membrane containing E1 and E2 glycoproteins and exhibits high genetic plasticity, which facilitates its adaptation to a broad range of hosts. The viral replication cycle begins with the fusion of the viral envelope to the host cell membrane, followed by translation of viral proteins and the assembly of new virions. MAYV is classified into three genotypes: D (dispersed), L (limited) and N (new), the latter identified in Peru (8-13). In addition to its sylvatic cycle, MAYV is proposed to establish urban transmission through vectors such as *Aedes*

92 *spp.*, *Culex spp.* and *Sabethes spp.*, with potential vertebrate reservoirs including
93 marsupials, rodents, birds and alligators (14-16).

94 Clinically, Mayaro disease is generally a self-limiting illness characterized by
95 fever, rash, headache, photophobia, myalgia and persistent polyarthralgia, which may last
96 for months or even years, significantly impacting patients' quality of life. Hemorrhagic
97 and neurological complications, as well as myocarditis, have also been reported (17). The
98 clinical similarity to other arboviral diseases, such as Dengue and Chikungunya,
99 combined with limited diagnostic capacity in endemic regions, hinders accurate
100 differential diagnosis and contributes to underestimation of the actual disease burden (18).
101 Beyond its typical acute presentation, increasing evidence from other arboviral infections,
102 including Zika and Chikungunya viruses (ZIKV; CHIKV), indicates that clinical
103 outcomes and transmission dynamics may extend beyond the classical vector-borne
104 paradigm, raising questions about the potential involvement of vulnerable populations
105 such as pregnant women and neonates (19-22). Although no specific antiviral treatments
106 or licensed vaccines are currently available, several vaccine candidates are under
107 development, with sustained epidemiological surveillance remaining essential to
108 anticipate and mitigate future outbreaks (3, 8, 23).

109 Animal models, particularly murine species, have been instrumental in elucidating
110 the pathogenesis of MAYV and in the preclinical evaluation of therapeutic and vaccine
111 candidates. These models faithfully reproduce hallmark clinical manifestations—
112 including ruffled fur, altered gait and ocular irritation—as well as key histopathological
113 features such as arthritis, myositis and tenosynovitis (24, 25). Disease outcomes vary
114 depending on host age and immune status (26-28). While the musculoskeletal system
115 represents the site of the most evident clinical damage, the liver and spleen act as major
116 systemic sites of viral replication, functioning as central hubs for Mayaro virus

117 amplification and dissemination (9, 27). The development of experimental platforms that
118 enable robust and reproducible antiviral testing is essential for advancing MAYV
119 research. In this context, the integration of *in vivo* imaging technologies constitutes a
120 major methodological advance, as it allows real-time, non-invasive monitoring of viral
121 dissemination dynamics using tagged viruses (26, 29).

122 Here, we establish and refine a murine model as a preclinical platform for the
123 future evaluation of antiviral drugs and therapeutic interventions against MAYV. To
124 validate early systemic dissemination under controlled conditions, we employed a
125 nanoluciferase-expressing MAYV reporter for longitudinal *in vivo* imaging.
126 Complementary experiments using wild-type MAYV were performed to characterize
127 tissue tropism, viral load, hematological and biochemical alterations and placental
128 transcriptional responses following controlled infection. We further assessed gestational
129 stage–dependent placental permissiveness and explored the biological plausibility of
130 vertical and sexual transmission. We hypothesize that gestational timing modulates
131 placental susceptibility to MAYV, defining critical windows of maternal–fetal
132 vulnerability. Together, this integrated framework provides a basis for mechanistic
133 investigation of systemic dissemination, reproductive involvement and maternal–fetal
134 risk during MAYV infection.

135 Materials and methods

136 Ethics statement

137 All procedures and experiments were conducted in accordance with the Ethics
138 Committee on Animal Use of the Institut Pasteur de Montevideo (CEUAIP #010-22, in
139 compliance with National Law 18.611 "Procedures for the Use of Animals in

140 Experimentation, Teaching and Scientific Research Activities") and strictly followed
141 ARRIVE guidelines.

142 MAYV infective clones

143 This study employed wild-type MAYV and nano Luc-expressing MAYV
144 (MAYV-nLuc) infectious clones based on the TRVL 4675 strain, a genotype D virus
145 originally isolated from a human case in Trinidad in the 1950s and kindly provided by
146 Dr. James Weger-Lucarelli (29-31).

147 Cell culture

148 Vero cells were maintained in Dulbecco's Modified Eagle Medium (DMEM)
149 supplemented with 10% fetal bovine serum (FBS), penicillin (100 U/mL) and
150 streptomycin (100 µg/mL) and maintained at 37 °C, with 5% CO_2.

151 Virus generation

152 Infectious virus was rescued from both WT and MAYV-nLuc infectious clones
153 by transfection of Vero cells using Lipofectamine™ 3000 (Invitrogen), according to the
154 manufacturer's instructions. Viral supernatants were collected when transfected cells
155 exhibited ≈80% cytopathic effect (CPE) and stored at -80°C as passage P0.

156 Working viral stocks were generated by sequential infection of Vero cells to produce P1
157 and P2 passages. The P2 viral stocks were titrated by plaque assay, verified by sequencing
158 and stored at -80°C until further use.

159 Mice

160 BALB/cJ mice (#000651) were bred and maintained at the Laboratory Animal
161 Biotechnology Unit's animal facility of Institut Pasteur de Montevideo. Mice were housed
162 in IVC Isolator Biocontainment unit (ISOCAGE-N, Tecniplast, Milan, Italy) and
163 acclimatized for one week prior to the experimental procedures. The cages were prepared
164 with wood chip bedding (Toplit 6, SAFE, France), plastic tunnels as enrichment and paper
165 napkins as nesting material. Environmental conditions were maintained at 20 ± 1°C, with
166 30–70% relative humidity and a 14/10-hour light/dark cycle. The mice were provided
167 with *ad libitum* autoclaved standard diet (D113, SAFE) and filtered autoclaved water.
168 Mice were specific pathogen-free (SPF) certified by IDEXX (USA) quarterly, in
169 accordance with FELASA standards.

170 Animal experimental design

171 Intraperitoneal (i.p.) inoculation was selected to enable controlled and
172 synchronized assessment of early systemic dissemination of Mayaro virus under
173 standardized experimental conditions. Although this route does not reflect natural
174 mosquito-borne transmission, it enables precise dose administration and reproducible
175 systemic exposure, thereby facilitating analysis of early viral dissemination dynamics. A
176 nanoluciferase-expressing MAYV reporter (MAYV-nLuc) was employed for non-
177 invasive *in vivo* imaging. This reporter-based approach was used to define spatial and
178 temporal dissemination patterns. Complementary experiments using wild-type MAYV
179 were subsequently performed to quantify systemic infectious viral loads, characterize
180 hematological and biochemical alterations and assess placental transcriptional responses
181 following controlled infection. Viral doses were optimized according to the specific
182 objectives of reporter-based imaging and pathogenesis studies. Sex-specific analyses
183 were incorporated where biologically relevant, including assessment of reproductive

184 tissue tropism and transmission experiments. This integrated experimental framework
185 enabled systematic evaluation of viral dissemination, reproductive involvement and
186 gestational stage–dependent placental permissiveness (Fig 1).

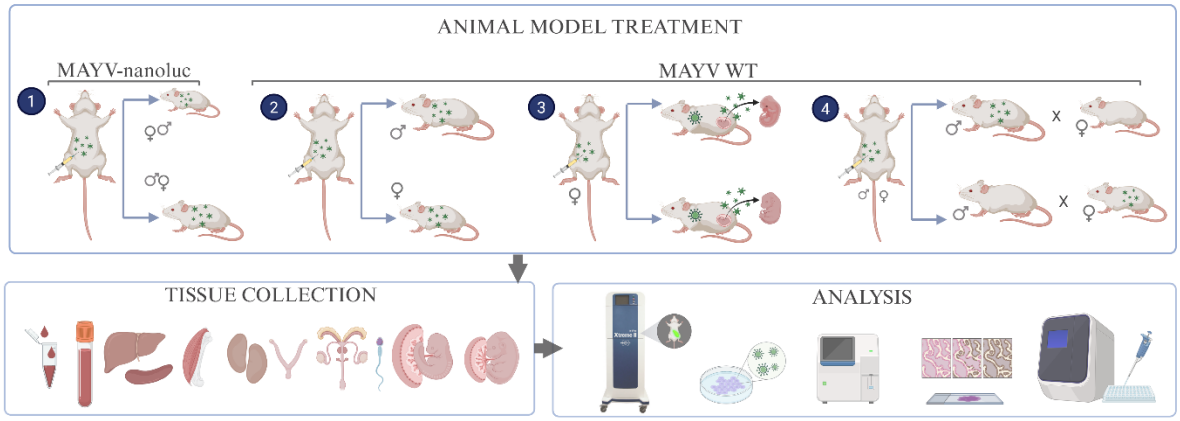

187

188 **Figure 1. Experimental design for longitudinal assessment of early systemic dissemination of Mayaro**
189 **virus in mice.** Mice were i.p. inoculated with a bioluminescent Mayaro virus to enable longitudinal, non-
190 invasive monitoring of early viral dissemination by *in vivo* imaging. Parallel groups were infected with
191 wild-type Mayaro virus to evaluate tissue tropism and transmission-related outcomes. Blood and lymphoid,
192 visceral, musculoskeletal and reproductive tissues were collected for downstream analysis.

193 *In vivo* imaging evaluation with MAYV-nLuc infection

194 *In vivo* bioluminescence imaging frequency was performed over a 10-day
195 observation window to capture the peak of viral replication and the onset of immune
196 responses associated with recovery from acute infection, based on previous reports (24,
197 25, 32). Age groups were selected according to their susceptibility to MAYV infection,
198 with younger animals exhibiting higher susceptibility (33). For this study, four- and eight-
199 week-old BALB/cJ female mice were i.p. infected with 1 x 10^4 PFU of MAYV-nLuc
200 resuspended in 100 µL PBS (n=4 per age group). Mock-infected animals received PBS
201 only (n = 2; one animal per age group). The viral dose was selected based on pilot
202 optimization experiments to ensure robust reporter detection while maintaining animal

203 welfare. To perform *in vivo* luminescence imaging, the animals were i.p. injected with 20
204 µg of Furimazine (TargetMol®, MA, USA) in 100 µL of PBS, anesthetized with
205 isoflurane (3–4% for induction and 1-2 % for maintenance) and imaged at defined time
206 points using an In-Vivo Xtreme II™ system (Bruker Daltonik GmbH, Billerica, MA,
207 USA). Image acquisition and analyses were performed using MolecularImaging software
208 V.7.5.3.22464 (Bruker Daltonik Gmbh, Billerica, MA, USA). Thresholds and exposure
209 times were kept constant across time points for longitudinal comparability.
210 Bioluminescent signal reflects reporter expression and may not directly correlate with
211 infectious viral titers. Imaging was performed at 1-, 2-, 6- and 10- day post infection (dpi).
212 Animals were necropsied at 6 dpi (n=2 per age group) and at 10 dpi (remaining animals).
213 Organs collected for confirmation of infectious viral particles included the liver, kidneys,
214 spleen and *quadriceps femoris* muscle. Peripheral tissues exhibiting luminescent signal—
215 tail, ear, forelimb or hindlimb—were also sampled.

216 Viral tropism of Mayaro WT and health status

217 Twelve BALB/cJ female and twelve BALB/cJ male mice (4 weeks old) were i.p. infected
218 with 1 x 10^5 PFU of MAYV WT resuspended in 100 µL of PBS (n=24). Mock-infected
219 mice received the PBS diluent alone (n=4). The viral dose was selected based on prior
220 pilot experiments as the lowest dose that consistently allowed detection of infectious viral
221 particles across tissues during acute infection. Blood samples were collected pre and post-
222 infection for hematological and biochemical parameter analyses at 0-, 24- and 48-hour
223 post infection (hpi). At 24 hpi, six animals of each sex were euthanized under deep
224 anesthesia induced by ketamine-xylazine mixture administered via the i.p. route
225 (ketamine 110 mg/kg; Pharmaservice, Ripoll Vet, Montevideo, Uruguay; xylazine 13
226 mg/kg; Seton 2%; Calier, Montevideo, Uruguay), followed by cervical dislocation.
227 Organs collected for quantification of infectious viral particles included the liver, kidneys,

228 spleen, *quadriceps femoris* muscle, ovaries, uterus, seminal vesicles and testes. The same
229 procedures were performed on the remaining animals at 48 hpi.

230 MAYV WT vertical transmission

231 Seventeen BALB/cJ female mice (8-weeks old) were synchronized in their estrous cycle
232 by exposing them to male dirty bedding for 72 h prior to mating (34). Mating was then
233 performed by placing one proven male in a cage with two females for 48 h and the
234 presence of a vaginal plug was checked daily from the following morning as a positive
235 sign of mating to be considered day 0.5 of pregnancy. At 7.5-8.5-day post-coitum (dpc),
236 six females were i.p. infected with 1 x 10^5 PFU of MAYV WT resuspended in 100 µL of
237 PBS, while two mock-infected received only PBS diluent (n = 6 infected; n = 2 mock).
238 The females were euthanized and necropsied at 48 hpi (9.5-10.5 dpc). Blood samples
239 were collected prior to euthanasia for post-infection hematological and biochemical
240 analyses. Organs collected for quantification of infectious viral particles and histological
241 analysis included the liver, kidneys, *quadriceps femoris* muscle, ovaries, uterus, placenta
242 and fetus. The same procedures were performed on the remaining pregnant females
243 infected at 13.5–14.5 dpc (n = 7 infected; n = 2 mock), which were necropsied at 48 hpi
244 (15.5-16.5 dpc).

245 MAYV WT sexual transmission

246 To evaluate sexual transmission in both directions, BALB/cJ mice were mated in a 1:1
247 ratio under controlled conditions. For female-to-male transmission, seven 8-week-old
248 females were synchronized in their estrous cycles by exposure to male dirty bedding for
249 72 h prior to mating, as described above and were infected i.p. with 1 × 10^5 PFU of MAYV
250 in 100 µL of PBS 12 h before pairing with uninfected males. For male-to-female
251 transmission, six synchronized 8-week-old females were paired with males infected i.p.

252 with the same viral dose and schedule. Infected animals were necropsied at 48 hpi,
253 whereas their uninfected partners at 48 h after mating. The liver, spleen, *quadriceps*
254 *femoris* muscle, ovaries, uterus, seminal vesicles and testes were collected for infectious
255 viral particle detection by plaque assay and for RT-qPCR analysis in organs from exposed
256 animals. Sperm from the bilateral cauda epididymides was collected for plaque assay and
257 RT-qPCR analysis. For analytical purposes, an exposed animal was defined as an
258 uninfected individual mated with an infected partner.

259 Hematology and biochemistry profile

260 For hematological analysis, 20 µL of blood per animal were collected and stored
261 in 0.5 mL microtubes containing potassium EDTA salts (W anticoagulant, Wiener Lab,
262 Rosario, Argentina) at a 1:10 ratio (EDTA: blood). Samples were analyzed using an Auto
263 Hematology Analyzer BC-5000 Vet (Mindray, Shenzhen, China). The parameters
264 evaluated included white blood cells (WBC), neutrophils (Neu), lymphocytes (Lym),
265 monocytes (Mon), eosinophils (Eos), basophils (Bas), red blood cells (RBC), hemoglobin
266 (HGB), hematocrit (HCT), mean corpuscular volume (MCV), mean corpuscular
267 hemoglobin (MCH), mean corpuscular hemoglobin concentration (MCHC) and platelets
268 (PLT).

269 For biochemical blood profile analysis, 100 µL of whole blood per animal was
270 collected and mixed with 0.5 µL of sodium heparin (Heparin Na, 20 U/mL). Using the
271 Chemistry Analyzer Pointcare® V3 (Tianjin MNCHIP Technologies Co. Ltd, Tianjin,
272 China), the following parameters were evaluated: total protein (TP), albumin (ALB),
273 globulin (GLO), total bilirubin (Tbil), alanine aminotransferase (ALT), aspartate
274 aminotransferase (AST), gamma-glutamyl transferase (GGT), blood urea nitrogen (BUN)
275 and creatinine (CRE).

276 # Tissue collection and processing

277 Samples collected from each organ of interest were weighed, rapidly frozen in
278 liquid nitrogen under a biosafety cabinet and stored at -80°C until processing. Samples
279 were homogenized using zirconium beads (0.5 mm/tube) and 800 µL of sterile 1× DPBS
280 in a Precellys® 24 homogenizer (Bertin Technologies, France), (2 min, power 10).
281 Homogenates were clarified by centrifugation (6,000 × g, 5 min) and supernatants were
282 stored at −80 °C for viral titration or RT-qPCR analysis.

283 # Viral titration

284 For viral titration, confluent Vero cell monolayers in 12-well plates (2.6×10^6
285 cells per plate) were inoculated with tissue homogenate–derived supernatants and their
286 10-fold serial dilutions (200 µL per well) and incubated at 37 °C with 5% CO_2 for 1 h,
287 with gentle rocking every 15 min to ensure uniform inoculum distribution. Mock-infected
288 wells served as negative controls. After adsorption, cells were overlaid with DMEM
289 containing 0.8% agarose, 1.6% FBS, penicillin and streptomycin and incubated for 48 h.
290 Monolayers were then fixed with 4% formaldehyde, stained with crystal violet and
291 plaques were counted to determine viral titers, expressed as plaque-forming units per
292 gram of tissue (PFU/g).

293 # Mouse sperm collection

294 The bilateral cauda epididymides were collected in a 60 mm plastic Petri dish and
295 incised with several cuts using fine scissors, releasing the sperm into a 50 µL drop of
296 Dulbecco's Phosphate Buffered Saline 1x (DPBS, Sigma-Aldrich) and stored at −80°C
297 until further processing. Later, sperm samples were thawed and resuspended in 150µL of
298 PBS. Zirconium beads were added to each sample and disruption was performed using a

299 Bullet Blender® STORM 24 (Next Advance Inc., New York, USA) for one minute at
300 speed 8. After centrifugation, 100 µL of supernatant was divided into two aliquots. To
301 assess the presence of MAYV, one aliquot was subjected to cell culture amplification
302 followed by plaque assay, whereas the other was analyzed directly for viral RNA by RT-
303 qPCR.

304 Viral RNA extraction and detection

305 Viral RNA from tissues was extracted from clarified tissue homogenate
306 supernatants, as described above, using the QIAamp® Viral RNA Mini Kit (QIAGEN),
307 according to the manufacturer's instructions. RNA from sperm samples was extracted
308 from TRIzol-treated homogenates using the Direct-zol RNA Miniprep Kit (Zymo
309 Research), following the manufacturer's guidelines. RNA samples were eluted in 25µL
310 of nuclease-free water and stored at -80ºC until further use (35). Detection was performed
311 using a one-step real-time reverse transcription PCR (RT-qPCR) assay, employing the
312 primers and probe listed in Table 1, which target an 86-bp region of the MAYV nsP1
313 gene. Reactions were carried out using TaqMan™ Fast Virus 1-Step Master Mix (Thermo
314 Fisher Scientific) on a QuantStudio™ 7 Pro Real-Time PCR System (Applied
315 Biosystems). Due to limited sample availability, sperm-derived RNA samples were
316 analyzed in technical duplicates. The assay was used for qualitative detection
317 (presence/absence) of viral RNA.

318 **Table 1: primers and probe used for MAYV detection by qPCR.**

MAY-qPCR-Fw	5'-AGGACCCAGAGGAACACTAATA-3'
MAY-qPCR-Rv	5'-CGATACTCTTTCGCCCACTTAC-3'

MAY-qPCR-Probe	5'-/56-FAM/TACCTGCTT/ZEN/CCAGTGGTGTCACAA/3IABkFQ/-3'

319

320 ## Cell culture–based isolation of virus from sperm samples

321 Due to the limited volume of sperm samples, processed samples were subjected
322 to passage in Vero cells to allow potential biological amplification prior to titration. Vero
323 cells were seeded in 96-well plates at 5,000 cells per well in 100 µL of DMEM
324 supplemented with 5% FBS, penicillin (100 U/mL) and streptomycin (100 µg/mL). The
325 following day, cells were inoculated with 100 µL of processed sperm samples. Mock-
326 infected wells receiving culture DMEM alone served as negative controls. After 72 h of
327 incubation at 37 ºC, supernatants were harvested and the presence of infectious viral
328 particles was assessed by plaque assay. Cytopathic effects were monitored using inverted
329 optic microscope Zeiss Primovert, Carl Zeiss Suzhou Co., LTD, China.

330 ## Transcriptomics in placenta

331 For the RNA-seq experiment, three placentas per condition (control uninfected;
332 infected at 7.5-8.5 dpc and infected at 13.5-14.5 dpc) were selected and processed for
333 total RNA extraction. Placentas stored at −80 °C were disrupted in TRI Reagent using a
334 Bullet Blender® STORM 24 (Next Advance Inc., New York, USA) with 0.5 mm
335 zirconium oxide beads (ZROB05, Next Advance Inc.) for 10 min at maximum speed.
336 Following homogenization, the samples were centrifuged to remove beads and debris.
337 The upper aqueous phase was collected and purified using the Direct-zol RNA kit (Zymo
338 Research, USA) according to the manufacturer's instructions. RNA was quantified with
339 RNA HS Qubit (Invitrogen, USA). RNA quality assessment, library construction and
340 sequencing were performed by Macrogen (Seoul, South Korea). Libraries were prepared

using TruSeq stranded total RNA with Ribo-Zero Gold kit (Illumina, USA). Sequencing was performed on an Illumina NovaSeq X platform. Paired-end reads of 100 base pairs were obtained.

Raw paired-end RNA-seq reads were aligned to the *Mus musculus* reference genome (GRCm39, Ensembl release 114) using STAR v2.7.8a. Aligned reads were quantified at the gene level using featureCounts v2.0.2 (Subread package). The Ensembl GTF annotation file (Mus_musculus.GRCm39.114.gtf) was used.

Downstream analysis was conducted in R v4.3.0 using the DESeq2 package. The raw count matrix was filtered to retain genes with a minimum of 10 total reads across all samples. A DESeq2 dataset was constructed with experimental conditions as the main design factor. Variance stabilizing transformation (VST) was applied to normalize data prior to visualization and clustering. Differential expression analyses were performed for multiple contrasts of interest and log2 fold changes were shrinkage-corrected using the "normal" method of lfcShrink. Genes with an adjusted p-value <0.05 were considered significantly differentially expressed.

Volcano plots were generated with ggplot2, where significant genes were highlighted (adjusted $p < 0.05$). Heatmaps of differentially expressed genes were created with pheatmap R package, using variance-stabilized expression values scaled by gene (row-wise z- scores). Color schemes were defined with the RColorBrewer package. Additional hierarchical clustering of differentially expressed genes was performed to assess global expression patterns across experimental groups. Gene ontology analysis was performed using Metascape (36).

Immunohistochemistry

364 Immediately after the necropsy, placenta and fetus from mid-stage of pregnancy were
365 fixed in 10% neutral buffered formalin (pH 7.4) for further processing. The samples were
366 then decalcified by immersion and agitation in a 3% aqueous nitric acid solution for 24
367 h. Once decalcification was complete, histological processing for paraffin embedding
368 began. Once the paraffin blocks were obtained from each sample, successive 4µm-thick
369 sections were made with a manual rotary microtome (Slee, Germany) and the successive
370 sections were mounted on slides and prepared for immunohistochemistry against MAYV
371 immunoreaction, using a rabbit polyclonal primary antibody (dilution 1:100) according
372 to a previous immunofluorescence protocol developed for immunocytochemistry in cell
373 cultures (37, 38). Histological and immunohistochemical blinded examinations were
374 performed using transmitted light microscope (Nikon Eclipse E200®, Nikon Corporation,
375 China) by two different veterinary pathologists.

376 Data Analysis

377 Statistical analyses were performed using GraphPad Prism version 10 (GraphPad
378 Software, San Diego, CA, USA). Viral load data (PFU/g) were $\log_{10}$-transformed prior to
379 analysis. Values below the limit of detection (LOD) were imputed as LOD/2 (630 PFU/g)
380 before transformation. Viral load data were analyzed using mixed-effects models
381 (REML), including time point, tissue, sex and their interactions as fixed effects and
382 individual animal as a random effect to account for within-subject variability. Post hoc
383 comparisons were performed using Tukey's multiple comparisons test. Hematological
384 and biochemical parameters with repeated measurements were analyzed using mixed-
385 effects models (REML), including time, infection status and their interaction as fixed
386 effects and individual animal as a random effect to account for within-subject correlation.
387 For cross-sectional analyses without repeated measures involving two factors (infection

status and gestational stage at 48 hpi), two-way ANOVA followed by Sidak's multiple comparisons test was used. Model assumptions were evaluated by assessing normality of residuals using the Shapiro–Wilk test and by visual inspection of residual plots. RNA-seq differential expression analysis was performed using DESeq2. Genes with fewer than 10 total counts across all samples were filtered out. Variance stabilizing transformation (VST) was applied prior to visualization and clustering. Differentially expressed genes were identified using adjusted p-values (Benjamini–Hochberg correction), with a significance threshold of adjusted $p < 0.05$. Data are presented as individual values with median lines for visualization, whereas statistical inference is based on model-derived estimates. All statistical tests were two-tailed and $p < 0.05$ was considered statistically significant.

Results

Bioluminescence reveals rapid dissemination and longitudinal persistence of MAYV-nLuc signal. Luminescence was first detected at 24 hpi (1 dpi) and remained detectable through the predetermined endpoint at 10 dpi. Signals were identified in the forelimbs, hindlimbs, tail, ears and abdominal region. The abdominal signal decreased after 6 dpi, whereas residual luminescence persisted in peripheral sites, remaining detectable mainly in the limbs at 10 dpi (Fig 2).

To assess the presence of infectious virus, plaque assays were performed on tissues collected at 6 and 10 dpi. Visceral organs (liver, spleen, muscle and kidneys) from both 4- and 8-week-old mice were analyzed, along with peripheral tissues (limbs, tail and ear) displaying detectable bioluminescent signal. In 4-week-old animals, infectious viral particles were recovered exclusively from peripheral tissues exhibiting luminescence including limb, tail and ear samples, whereas all visceral organs remained negative. Viral

loads in these peripheral compartments ranged from 1.49×10^3 to 2.98×10^5 PFU/g, with the highest titers detected in tail and limb tissues. In contrast, no infectious viral particles were detected in any tissues from 8-week-old animals, including peripheral tissues exhibiting bioluminescent signal.

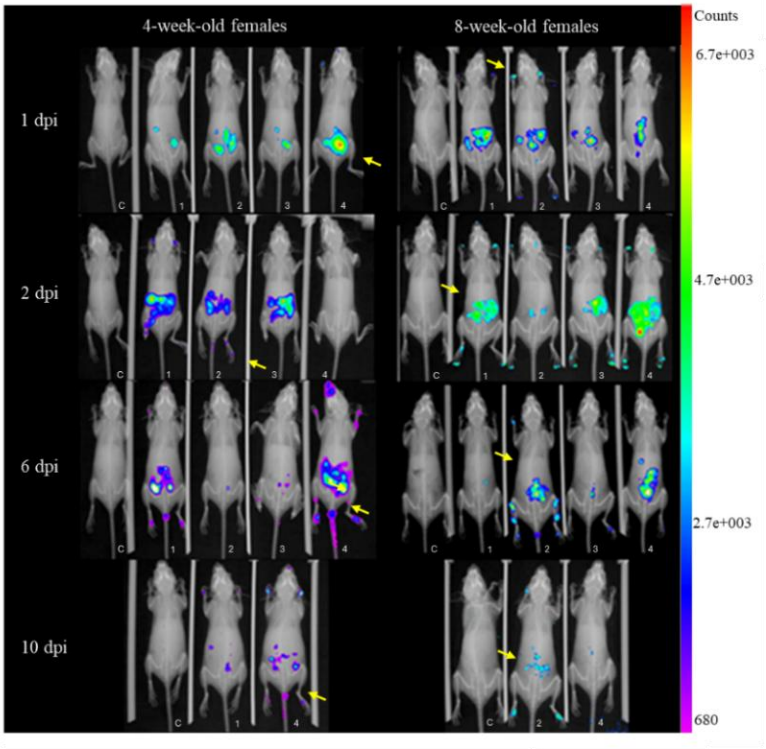

Figure 2. *In vivo* bioluminescence imaging of MAYV-nLuc infection in females at 4 and 8 weeks-old following i.p. inoculation (representative image). Luminescent signals (yellow arrows) were detected in the limbs, tail, ears and abdominal region at 1 (24 hpi), 2 (48 hpi), 6 and 10 dpi. Abdominal signals declined after 6 dpi, whereas residual luminescence persisted mainly in the limbs at later time points. Images from all animals in each age group are shown. All images were acquired and displayed using identical exposure settings and a fixed color scale to enable direct comparisons over time. C, mock-infected control.

Temporal dynamics and tissue tropism of MAYV infection in 4-week-old mice. Viral titers exhibited time- and tissue-dependent differences during acute infection (Fig 3A). Mixed-effects analysis with Tukey's multiple comparisons identified a significant increase in seminal vesicles at 48 hpi compared with 24 hpi (Mean difference

427 = 0.9452, SE of difference = 0.3397, p = 0.0284). Model-based estimates are reported as
428 mean differences (± SE), while graphical representations show individual values with
429 median lines due to non-normal data distribution. At 24 hpi, no significant inter-tissue
430 differences were detected, consistent with a relatively homogeneous early dissemination
431 pattern. By 48 hpi, tissue-specific differences emerged, with spleen titers exceeding those
432 in liver (Mean difference = 0.8391, SE of difference = 0.2150, p = 0.0352) and muscle
433 (Mean difference = 1.257, SE of difference = 0.2840, p = 0.0156). This substantial
434 difference suggests the spleen as a primary site of viral accumulation compared to
435 muscular tissue.

436 Sex-based analyses revealed transient differences at 24 hpi (Fig 3B). Specifically,
437 significant female–male differences were observed in the spleen (mean difference =
438 1.593, SE of difference = 0.5278, p = 0.0109) and kidneys (mean difference = 2.038, SE
439 of difference = 0.4765, p = 0.0159). In both tissues, males exhibited substantially higher
440 viral titers than females at this time point. Organ-specific viral distribution also varied
441 within each sex at 24 hpi. Among females, viral loads in the kidneys were significantly
442 higher than in the muscle (mean difference = 1.078, SE of difference = 0.2911, p =
443 0.0493). Conversely, in males, the spleen showed a significantly greater viral burden
444 compared to the liver (mean difference = 0.5601, SE of difference = 0.1205, p = 0.0205).
445 By 48 hpi, no significant differences in viral loads were observed either between sexes or
446 among tissues within each sex (Fig 3C). This lack of statistical significance ($p > 0.05$ for
447 all comparisons) indicates that the early sex-dependent effects and tissue-specific
448 disparities observed at 24 hpi are not sustained as the infection progresses toward later
449 stages.

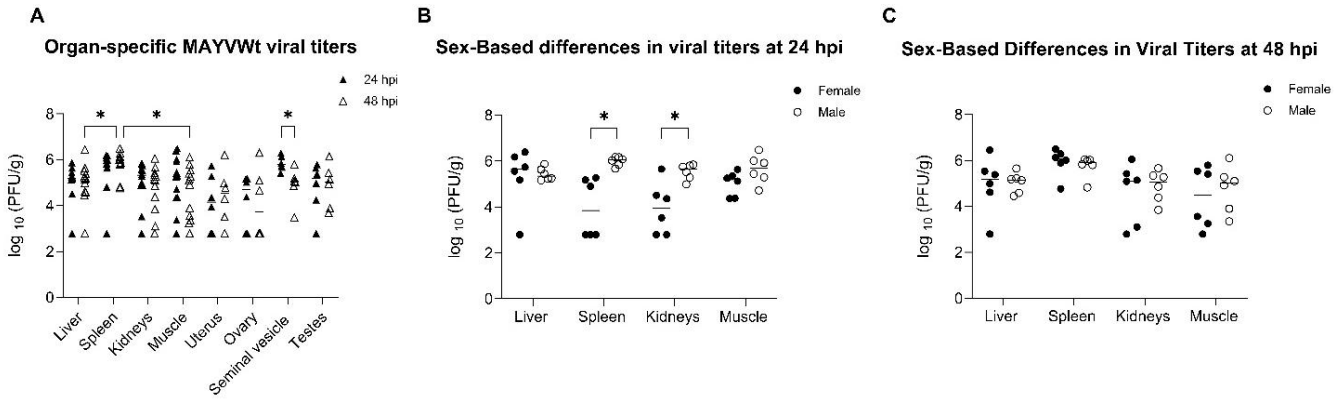

Figure 3. **Early systemic dissemination with time-dependent tissue tropism and transient sex effects.** Viral loads (log_{10} PFU/g) across tissues at 24 and 48 hours post-infection (hpi) and sex-based comparisons at each time point. (A) Viral loads across tissues at 24 and 48 hpi. (B) Sex-based comparison of viral loads across tissues at 24 hpi. (C) Sex-based comparison at 48 hpi. Viral loads were analyzed using mixed-effects models (REML) with time point and tissue as fixed effects and individual animal as a random effect, followed by Tukey's multiple comparisons test. Values below the limit of detection were assigned a value of LOD/2 (630 PFU/g) prior to transformation. Each dot represents an individual animal; horizontal lines indicate median values. Only statistically significant comparisons are indicated. Statistical significance was defined as $p < 0.05$ (*), $p < 0.01$ (**) and $p < 0.001$ (***).

Early hematological alterations during acute MAYV infection.

Hematological analysis revealed alterations in leukocyte profiles during acute infection. Total white blood cell counts (WBC) decreased trend at 24 and 48 hpi, accompanied by increased neutrophil (NEU) and decreased lymphocyte (LYM) percentages (Fig 4A–C). Platelet counts (PLT) showed a decreased at both time points although variability across animals was observed (Fig 4D). Eosinophils (EOS) decreased, basophils (BAS) increased at 48 hpi and monocytes (MON) remained stable in infected animals but decreased in mock controls (Fig S1A–C). Red blood cell counts (RBC) increased at 48 hpi, while hemoglobin (HGB) and hematocrit (HCT) increased at both time points (Fig S1D–F). Mean corpuscular volume (MCV) increased at 24 and 48 hpi, mean corpuscular hemoglobin (MCH) increased at 24 hpi and mean corpuscular hemoglobin concentration (MCHC) remained unchanged (Fig S3A–C). Red cell distribution width (RDW-CV and

RDW-SD) decreased at both time points. Mean platelet volume (MPV) increased, while platelet distribution width (PDW) decreased at 48 hpi. Procalcitonin (PCT) decreased in infected animals without changes in mock controls (Fig S3D–H). Statistically significant differences are indicated in the corresponding figures.

In biochemical and metabolic parameters, we observed that: Aspartate transaminase (AST) at both 24 and 48 hpi and increased alanine transaminase (ALT) at 48 hpi (Fig 4E–F). Creatinine (CRE) remained stable, whereas blood urea nitrogen (BUN) decreased at 24 hpi and showed a decreasing trend at 48 hpi, including in mock animals (Fig S1G–H). Total protein (TP) decreased at 48 hpi, while albumin (ALB), globulin (GLO) and gamma-glutamyl transferase (GGT) remained unchanged (Fig S2A–C, E). Total bilirubin (TBIL) decreased at 24 hpi (Fig S2D). Glucose (GLU) increased at both time points and body weight (BW) decreased at 24 and 48 hpi (Fig S2G–H). Statistical significance is indicated in the corresponding figures.

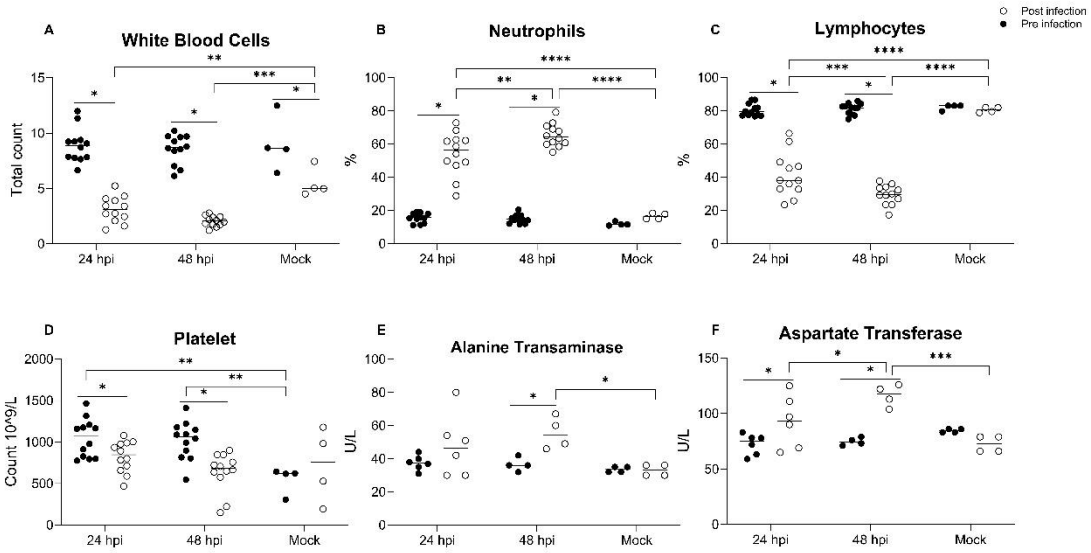

Figure 4. Early hematological and hepatic changes following acute MAYV infection. Hematological and hepatic parameters during acute MAYV infection at 24 and 48 hours post-infection (hpi) compared with mock controls. (A) Total white blood cell (WBC) count, (B) neutrophil percentage (NEU), (C) lymphocyte percentage (LYM), (D) platelet count (PLT), (E) alanine transaminase (ALT) and

490 (F) aspartate transaminase (AST). Each dot represents an individual animal; horizontal lines indicate
491 median values. Statistical analyses were performed using mixed-effects models (REML) for repeated
492 measures with time and condition as fixed effects and individual animal as a random effect. Differences
493 were considered statistically significant at $p < 0.05$ (*), $p < 0.01$ (**) and $p < 0.001$ (***).

494 **Gestational stage–dependent differences in MAYV distribution during**
495 **pregnancy.** At 48 hpi, viral titers exhibited significant variations based on gestational
496 stage across multiple tissues (Fig 5). Mixed-effects modeling followed by Tukey's
497 multiple comparison test revealed significantly higher infectious viral loads at 48 hpi in
498 tissues analyzed at 15.5–16.5 dpc (pregnant mice infected at 13.5-14.5 dpc) compared
499 with those analyzed at 9.5–10.5 dpc (pregnant mice infected at 7.5-8.5 dpc). This stage-
500 dependent increase was observed in the spleen (mean difference = 0.5751, SE of
501 difference = 0.1624, p = 0.0213), liver (mean difference = 1.924, SE of difference =
502 0.1552, p = 0.0011), kidneys (mean difference = 1.691, SE of difference = 0.3097, p =
503 0.0055), uterus (mean difference = 1.660, SE of difference = 0.6606, p = 0.0403) and
504 placenta (mean difference = 0.7328, SE of difference = 0.2277, p = 0.0061). However,
505 infectious virus remained undetectable in fetal tissues at this same stage (15.5–16.5 dpc),
506 with titers falling below the limit of detection. This suggests that even when the placenta
507 is significantly infected, the virus remained undetectable at the fetal compartment in an
508 infectious form. Within early gestation (9.5–10.5 dpc), tissue-specific differences were
509 observed, with the spleen showing higher titers than the liver and kidneys. At mid-
510 gestation, infectious viral particles remained detectable in maternal and placental
511 compartments, supporting ongoing systemic dissemination despite restricted recovery of
512 infectious virus from fetuses.

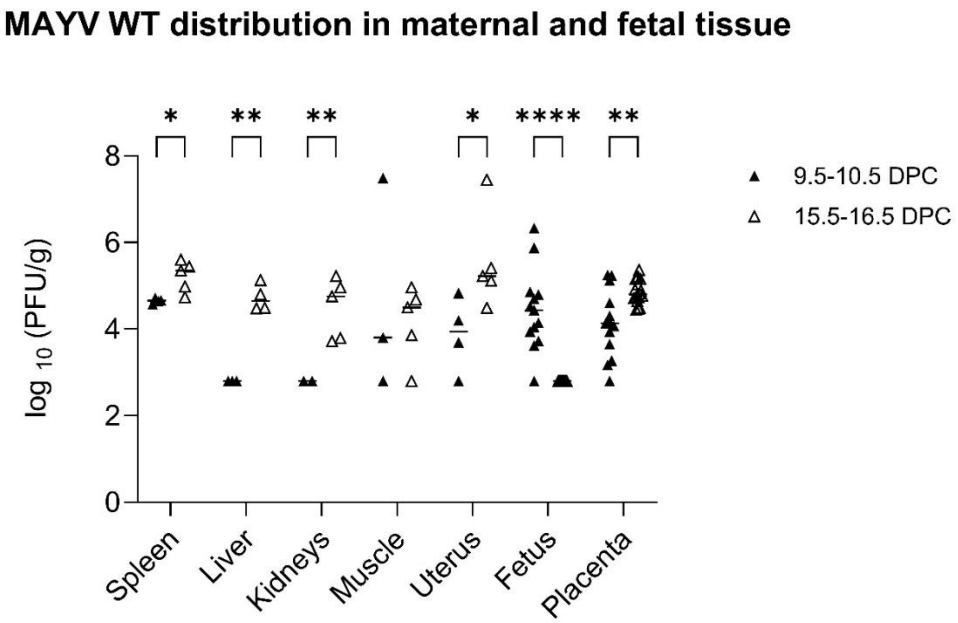

Figure 5. Gestational stage shapes maternal–fetal distribution and restricts recovery of infectious virus from mid-gestation fetuses. Infectious viral loads (log_{10} PFU/g) in maternal and fetal tissues at 48 hours post-infection (hpi) according to gestational stage. Females were infected at early (7.5–8.5 dpc; analyzed at 9.5–10.5 dpc) or mid-gestation (13.5–14.5 dpc; analyzed at 15.5–16.5 dpc). Each dot represents an individual animal; horizontal lines indicate median values. Viral loads were analyzed using mixed-effects models (REML) with gestational stage and tissue as fixed effects and individual animal as a random effect, followed by Tukey's multiple comparisons test. Values below the limit of detection were assigned a value of LOD/2 (630 PFU/g) prior to transformation. Only statistically significant comparisons are indicated. Statistical significance was defined as $p < 0.05$ (*), $p < 0.01$ (**) and $p < 0.001$ (***).

Exploratory analysis of hematological parameters at 48 hpi revealed alterations in leukocyte profiles across gestational stages. Infected females at both gestational stages exhibited higher neutrophil and lower lymphocyte percentages compared with mock controls (Fig S4A–B). Total white blood cell (WBC) counts were reduced in infected animals (Fig S4C). Platelet (PLT) counts showed variability between groups without a consistent pattern across gestational stages, while red blood cell (RBC) counts and procalcitonin (PCT) levels remained comparable (Fig S4D–F). Given the

530 limited number of mock controls, comparisons involving these groups should be
531 interpreted with caution.

532 **Immunohistochemistry confirms placental and fetal localization of**
533 **MAYV at mid stage.** Immunohistochemical analysis revealed clear differences in
534 MAYV antigen distribution between infected and non-infected placental and fetal tissues.
535 In placentas from infected females, moderate granular cytoplasmic staining was observed
536 in a substantial proportion of giant trophoblast cells within the maternal–fetal junction
537 zone (basal plate), indicating focal placental infection. In contrast, placentas from non-
538 infected pregnant females showed only nonspecific erythrocyte staining and otherwise
539 negative to mild background labeling. In fetuses from infected females, intense
540 immunostaining was detected across multiple organs, particularly in the intestinal visceral
541 epithelium, developing bone (growth cartilage) and other collagen-rich tissues, including
542 cartilage and dermis. Calcified bone exhibited no staining or only minimal labeling in
543 both intensity and extent. Fetuses from non-infected females were largely negative,
544 showing only nonspecific erythrocyte staining and minimal background labeling in
545 collagen-rich tissues (Fig 6).

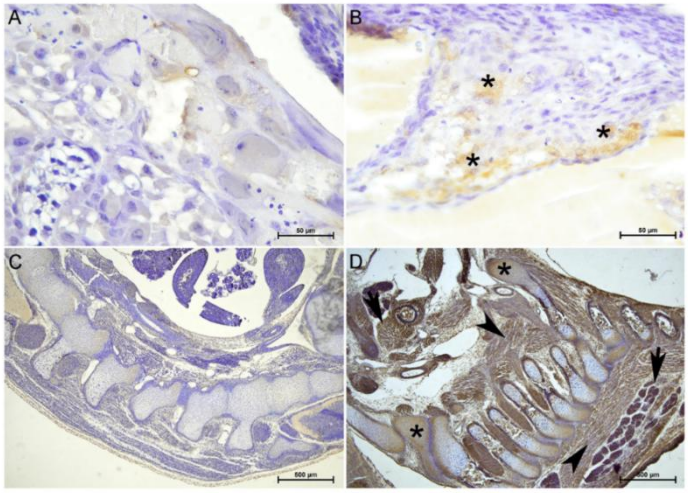

546

547 **Figure 6. IHC against MAYV**. A) Placenta of an uninfected mouse (control): Negative to mild (-/+)
548 immunostaining of isolated trophoblasts (foam giant cells) from the basal plate of the maternal-fetal
549 junction is observed. Scale bar = 50µm, 40×. B) Placenta of an experimentally infected mouse: Mild to
550 moderate, granular intracytoplasmic staining of foci of trophoblasts (foam giant cells) from the basal plate
551 of the maternal-fetal junction is observed (asterisks). Scale bar = 50µm, 40×. C) Fetus of the same
552 uninfected mouse of Figure A: No immunostaining against MAYV is observed (-). Scale bar = 500µm, 4×.
553 D) Fetus of the same experimentally infected mouse of Figure B: There is intense immunostaining in several
554 organs, particularly in uncalcified developing bone and growth cartilage (asterisks), as well as other
555 collagen-rich tissues (cartilage and dermis) (arrowheads) and the perimysium of skeletal muscles (arrows).
556 Already calcified bone shows no staining or minimal staining in intensity and extent. Scale bar = 500µm,
557 4×.

558 **Placental transcriptional responses to MAYV are gestational stage-**
559 **dependent.** To investigate placental transcriptional responses to MAYV infection,
560 differential gene expression was performed. The profiles revealed gene expression
561 patterns influenced by viral infection at early and mid-stages: 208 genes were upregulated
562 and 60 downregulated at the early stage and 139 genes were upregulated and 1
563 downregulated at the mid stage (Fig 7A and Table S1). Among the upregulated genes, 50
564 were shared between both stages, leaving 158 stage-specific upregulated genes at the
565 early stage and 89 at the mid stage. These data suggest a robust transcriptional response
566 to infection during the early stage of pregnancy, while the response in mid pregnancy,
567 although sharing common pathways, is comparatively attenuated.

568 Gene Ontology (GO) enrichment analysis of the 50 shared upregulated genes revealed
569 significant association with antiviral defense pathways, including responses to viral
570 infection, interferon-stimulated genes (ISGs) activity and cytokine-mediated signaling
571 (Fig 7B).

572 The 158 genes uniquely upregulated in the early stage were enriched not only for the
573 immune pathways but also for distinct biological processes, including heart development,
574 myeloid cell development, regulation of plasminogen activation, connective tissue
575 development and adipogenesis (Fig 7C). In contrast, the 89 late-stage-specific
576 upregulated genes were again predominantly associated with immune functions,
577 specifically type II interferon signaling, negative regulation of innate immune response
578 and innate antiviral immune response (Fig 7D).

579 Finally, GO analysis of the 60 genes downregulated specifically at the early stage
580 identified enrichment for processes such as multi-organism reproductive process, antigen
581 processing and presentation of peptide antigen via MHC class I, lymphocyte activation,
582 signaling by NTRKs, insulin secretion, thermogenesis, extracellular matrix organization
583 and adrenergic signaling in cardiomyocytes (Fig 7E).

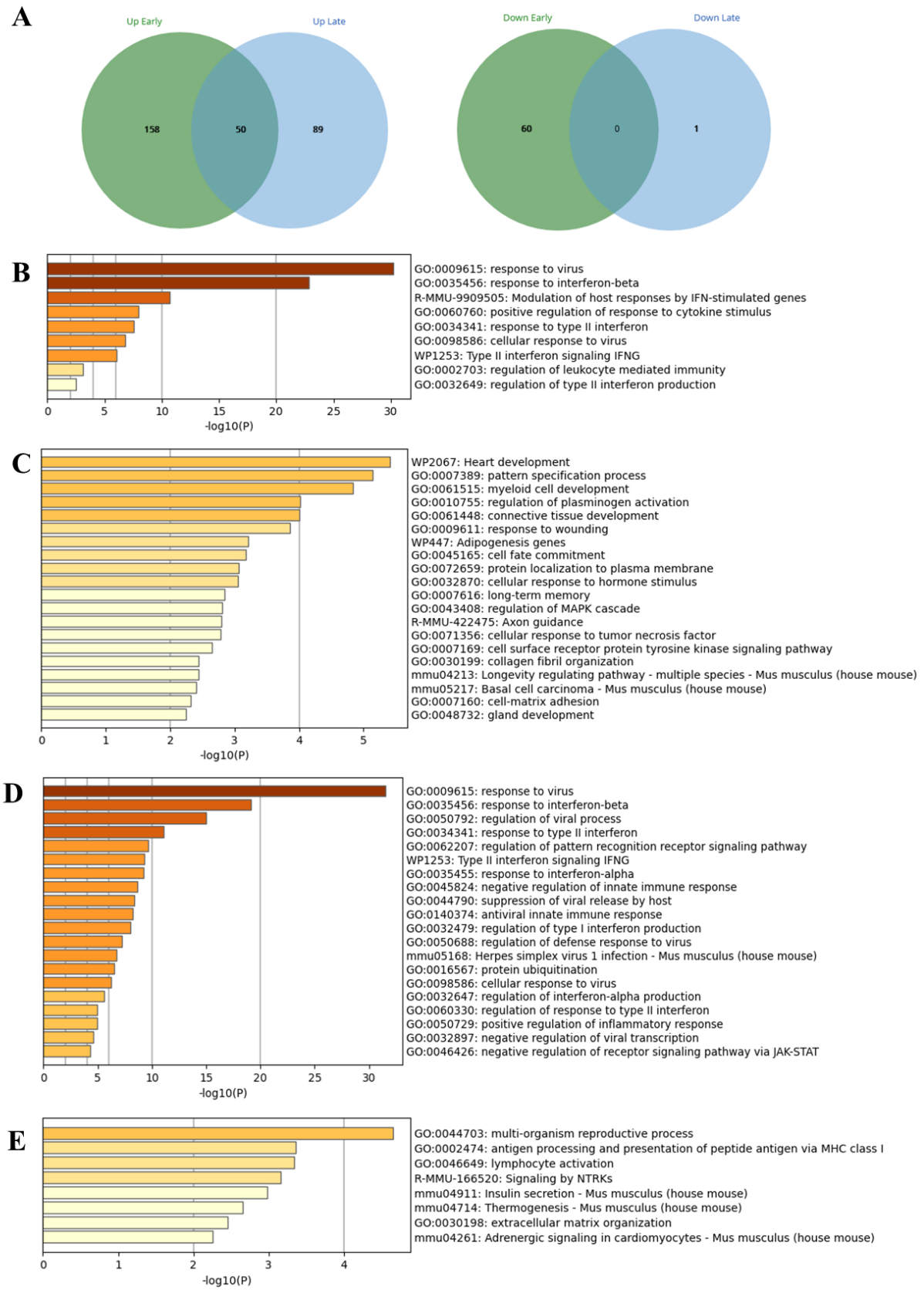

Figure 7. Transcriptomic profiles and Gene Ontology enrichment of placental response to MAYV infection at early and mid-gestational stages. A) Comparison of placentas infected at 7.5–8.5 dpc (early)

587 and 13.5–14.5 dpc (mid) versus controls revealed 208 up-/60 down-regulated genes at early stage and 139
588 up-/1 down-regulated at mid stage, with 50 genes shared between stages. B) Shared genes were enriched
589 for antiviral and interferon-mediated responses. C) Early-stage-specific genes were associated with
590 immune, developmental and metabolic pathways. D) Mid-stage-specific genes were mainly related to type
591 II interferon and innate immune modulation. E) Early-stage down-regulated genes were enriched for
592 reproductive, metabolic and signaling processes.

593 **MAYV detection in reproductive tissues and sperm.** Following mating, the
594 liver, spleen, *quadriceps femoris* muscle, ovaries, uterus, seminal vesicles and testes were
595 analyzed for the presence/absence of MAYV by plaque assay in all animals. RT-qPCR
596 was performed on the spleen of infected animals and on the corresponding organs from
597 exposed animals. To detect the presence/absence of MAYV in sperm, RT-qPCR was
598 performed and following cell culture amplification and plaque assay.

599 Infectious viral particles were detected in the spleen (7/7), ovaries (3/7) and muscle (1/7)
600 of infected females mated with uninfected males. In contrast, all organs analyzed from
601 exposed males were negative by both plaque assay and RT-qPCR. However, after cell
602 culture amplification of sperm samples followed by plaque assay, infectious virus was
603 detected in one exposed male (1/7), which had been paired with the female positive for
604 infectious virus in both the spleen and muscle.

605 In infected males mated with uninfected females, infectious viral particles were
606 consistently detected in the testes (6/6) and in the spleen (3/6). Plaque assays performed
607 after cell culture amplification of sperm revealed infectious virus in four males (4/6),
608 consistent with the cytopathic effect observed (Fig 8). Viral RNA was also detected by
609 RT-qPCR in direct unamplified sperm samples from the same four animals. No infectious
610 virus was detected in the seminal vesicles. Among exposed females, infectious viral

611 particles tested positive in two animals: the uterus and ovary of one female and the spleen
612 of another, although the RT-qPCR resulted below the limit of detection.

613 Overall, viral detection in exposed animals was limited and inconsistent across analytical
614 approaches.

615 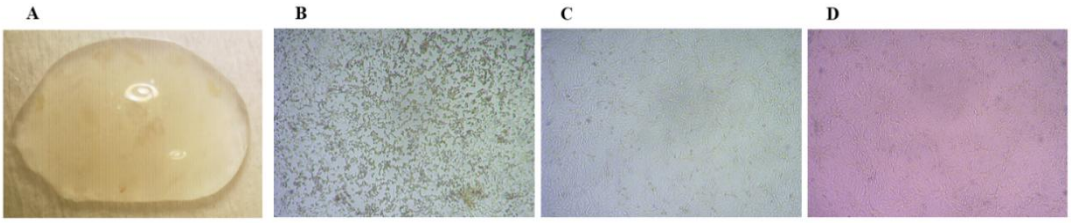

616 **Figure 8. Cytopathic effect of MAYV in sperm cell culture–based amplification** (Representative
617 image)**.** (A) Sperm extracted from the bilateral cauda epididymides. (B´D) Representative images of Vero
618 cells inoculated with processed sperm samples showing a MAYV-positive sample (B) a MAYV-negative
619 sample (C) and Mock-infected Vero cells (D). Cell morphology was examined by a Zeiss Primovert
620 inverted light microscope (40×).

621 # Discussion

622 Elucidating the tissue tropism and viral dynamics of MAYV is essential given the
623 limited evidence available for this emerging arbovirus and the relevance of murine
624 models for characterizing infection *in vivo*. Here, we provide evidence of MAYV
625 dissemination to fetal tissues in mice, identifying anatomical targets not previously
626 described. Together, these findings support a model in which gestational timing critically
627 determines placental permissiveness and fetal exposure to MAYV, identifying early
628 gestation as a window of heightened vulnerability during acute infection. Although direct
629 temporal equivalence between murine and human gestation is not possible, early murine
630 gestation (7.5-8.5 dpc) represents a developmental window of active placentation and
631 early organogenesis that broadly parallels the first trimester of human pregnancy, whereas

632 mid-gestation (13.5-14.5 dpc) reflects a more mature placental interface (21,40).
633 Considering that related alphaviruses may cross the placental barrier, our results
634 underscore the importance of including pregnancy models when assessing MAYV
635 transmission routes (41).

636 To examine early dissemination under controlled conditions, we employed a
637 nanoluciferase-expressing MAYV reporter to evaluate intraperitoneal delivery as a
638 strategy to achieve systemic exposure. *In vivo* imaging showed rapid and sustained viral
639 spread, with peripheral luminescent patterns consistent with the musculoskeletal
640 involvement previously described in experimental models and human disease (18,25,29).

641 The incomplete overlap between bioluminescent signal and recovery of infectious virus,
642 particularly in older animals, likely reflects differences in analytical sensitivity between
643 reporter-based imaging and plaque assays, the latter requiring a minimum threshold of
644 viable, replication-competent virions, as well as the persistence of viral material
645 following partial clearance. This is consistent with a temporal decrease in viral load over
646 time, suggesting progressive viral clearance despite persistent luminescent signal. In
647 contrast, the consistent recovery of infectious virus in younger mice supports age-
648 dependent variation in susceptibility and viral maintenance within target tissues.

649 This imaging approach enabled longitudinal, non-invasive monitoring of viral dynamics
650 over a 10-day period, encompassing both acute infection and early recovery phases (24,
651 25). By providing temporal and anatomical resolution of dissemination events that are
652 difficult to capture in natural transmission settings, the model links viral spread to
653 measurable tissue outcomes.

654 Together, these observations expand the experimental landscape for MAYV research,
655 supporting mechanistic investigations of tissue tropism, host responses and transmission

656 potential under standardized conditions and offering a framework for future studies
657 addressing reproductive involvement and non-vector routes of spreading.

658 MAYV WT exhibited rapid and systemic dissemination at 24 and 48 hpi, with
659 infectious virus detected across multiple organs during the acute phase, including
660 detection in reproductive tissues of pregnant females. These results are consistent with
661 other murine alphavirus models, including IFNAR−/− mice, in which widespread viral
662 detection at early time points reflects acute viremia (27). This pattern reflects an initial
663 homogeneous dissemination phase at 24 hpi followed by the emergence of tissue-specific
664 viral accumulation at 48 hpi, consistent with previous murine MAYV models showing
665 that viral burden is influenced by host age, immune status and route of infection, with
666 predominant viral accumulation in skeletal muscle, limbs and lymphoid organs such as
667 the spleen (9, 32). Infectious particles were also detected in muscle, supporting the
668 myopathy and myositis previously described during MAYV infection (9, 24, 28). The
669 increase in viral load in seminal vesicles at 48 hpi further supports progressive
670 involvement of reproductive tissues during acute infection, consistent with the detection
671 of infectious virus in male reproductive organs.

672 The early hematological shifts observed in our study partially align with previous
673 experimental and clinical reports of MAYV infection. In IFNAR−/− mice model, early
674 leukopenia predominantly driven by lymphopenia was reported during acute infection
675 (28), consistent with the trend toward leukopenia and lymphocyte reduction detected in
676 our model. In contrast, a BALB/c intraplantar infection model described increases in
677 monocytes, neutrophils and lymphocytes during the acute phase (24), indicating that
678 hematological profiles may vary depending on experimental conditions. In human cases,
679 leukopenia, thrombocytopenia and elevated ALT and AST have been documented among

680 reported laboratory abnormalities (17), which parallels the transient cytopenias and
681 aminotransferase elevations observed here. Together, these comparisons suggest that
682 early systemic hematological and biochemical changes are consistent with previously
683 reported features of MAYV infection, although their magnitude and direction may differ
684 across models and clinical settings. Despite the limited mock sample size in pregnant
685 cohorts, the observed shift in leukocyte distribution at 48 hpi across gestational stages
686 consistent with an early systemic inflammatory response rather than a global
687 hematological impairment.

688 MAYV belongs to the Alphavirus genus (17, 32), which includes viruses capable
689 of affecting the nervous system and embryonic development. The detection of infectious
690 particles in reproductive organs (uterus, ovary, testes, seminal vesicles), with variable
691 detection across tissues at both time points highlights a tissue tropism previously
692 described in immunodeficient mice (14) and raises the possibility of sexual or vertical
693 transmission. Transient and early sex-based differences were observed at 24 hpi. These
694 differences were no longer evident at 48 hpi. While most studies focused on age and
695 nutritional status as determinants of disease outcome (24, 29, 39), these observations
696 suggest a potential sex-dependent component of MAYV infection that warrants further
697 investigation, particularly given similar findings reported for CHIKV (40).

698 A gestational stage–dependent susceptibility was evident in our model. At the early stage
699 of pregnancy (7.5–8.5 dpc infection; analyzed at 9.5–10.5 dpc), fetuses contained
700 infectious particles at 48 hpi, indicating that MAYV can cross the maternal–fetal barrier
701 during acute infection. In contrast, our data suggest a more restrictive placental
702 environment during mid-gestation (13.5–14.5 dpc; analyzed at 15.5–16.5 dpc), as no
703 infectious particles were recovered from fetal tissues despite significant placental viral

704 loads. It is critical to interpret this 'restriction' specifically as the absence of infectious
705 viral particles detectable by plaque assay. While this confirms a lack of replication-
706 competent virions in the fetus at this stage, it does not preclude the potential presence of
707 viral RNA or non-infectious antigens that might be detectable through more sensitive
708 molecular methods. This is supported by our immunohistochemistry results, where viral
709 antigen was detected in fetal tissues at mid-gestation despite the absence of recoverable
710 infectious virus, suggesting either focal infection below the limit of detection or the
711 persistence of viral antigens following partial viral clearance. This timing-dependent
712 susceptibility is consistent with observations from ZIKV infection, where placental
713 infection and transplacental transmission are strongly associated with maternal infection
714 occurring during the first trimester of human pregnancy, whereas infections acquired at
715 later gestational stages are less frequently linked to fetal exposure (19, 41). This
716 window—analogous to early human embryogenesis (42) — displayed a broad
717 transcriptional response (208 upregulated, 60 downregulated genes), including alterations
718 in developmental and tissue-remodeling programs, as well as downregulation of
719 hormonal signaling, MHC I presentation and ECM organization. These disruptions are
720 compatible with teratogenesis described for alphaviruses such as Semliki Forest virus
721 (39) and ZIKV (20).

722 In contrast, at mid-gestation infection (13.5–14.5 dpc), infectious viral particles were not
723 detected in fetuses and transcriptional activation was more restricted (139 upregulated, 1
724 downregulated), dominated by interferon-mediated pathways. This profile aligns with
725 increased placental maturity and antiviral competence (20). The presence of infectious
726 viruses in placenta and uterus, but not in fetal tissues, supports restricted fetal infection at
727 this stage (42, 43). Together, these findings support the concept of a conserved gestational
728 window of vulnerability to vertical transmission among arboviruses, in which early

729 placentation is associated with increased permissiveness at the maternal–fetal interface.
730 The 50 shared upregulated genes across gestational stages—mostly ISGs—reflect a
731 conserved antiviral signature, but timing-dependent transcriptional divergence
732 underscores critical periods of vulnerability, including disruption of angiogenic and
733 developmental pathways (44) and inflammatory responses characteristic of MAYV (24,
734 25). Viral antigen was detected by immunohistochemistry in placental and fetal tissues at
735 mid-gestation, despite the absence of recoverable infectious virus, suggesting focal or
736 low-level infection below plaque assay detection limits or persistence of viral antigens
737 following partial viral clearance.

738 While direct extrapolation from murine models to humans is limited, these findings
739 provide a biologically plausible framework to explore potential maternal–fetal risks with
740 MAYV infection in human during pregnancy.

741 Limitations should be considered when interpreting these findings. Intraperitoneal
742 inoculation does not fully recapitulate natural mosquito-borne transmission and may
743 influence early viral kinetics. However, this route is widely used in murine models of
744 systemic arbovirus infection and was deliberately selected to enable controlled
745 assessment of early systemic dissemination and tissue tropism while minimizing
746 procedure-related distress (45, 46) and local inflammatory confounders. Although
747 intraplantar models better reproduce articular manifestations (24, 25, 27), intraperitoneal
748 delivery provides a standardized framework to evaluate systemic viral dynamics.

749 Previous murine studies have reported systemic MAYV dissemination and
750 detection of viral RNA in gonadal tissues, suggesting broader tissue distribution (47),
751 although evidence supporting a functional role of reproductive infection in transmission
752 has remained indirect. In the present study, infectious virus was detected in reproductive

753 organs and sperm, supporting the biological plausibility of sexual transmission, though
754 not establishing it as an efficient route and therefore requiring dedicated follow-up
755 studies. Consistent with this, detection among exposed animals was limited and
756 inconsistent, suggesting minimal or transient exposure rather than sustained transmission.
757 If sexual transmission occurs, it is likely to involve low-level infection and restricted
758 replication within gonadal tissues, potentially limiting detectability and contributing to
759 the scarcity of documented cases, a challenge also described for other arboviruses in
760 semen (42).

761 Taken together, these findings broaden the understanding of MAYV pathogenesis
762 by integrating virological, transcriptomic, histological and imaging approaches within a
763 unified murine model. We provide evidence of expanded tissue tropism, including
764 reproductive and fetal involvement and identify gestational timing as a determinant of
765 placental permissiveness and fetal exposure. Detection of infectious virus in reproductive
766 tissues supports the biological plausibility of non-vector transmission, although its
767 epidemiological relevance remains uncertain. While extrapolation to humans requires
768 caution, these results establish a preclinical framework for investigating MAYV systemic
769 dissemination, maternal–fetal infection and potential transmission routes.

770 Conclusion

771 This study establishes a murine model of MAYV infection that reveals rapid
772 systemic dissemination followed by tissue-specific viral distribution, broad tissue tropism
773 and early involvement of reproductive organs. Transient sex-dependent differences were
774 observed during the early phase of infection, suggesting a potential but limited role of sex
775 in modulating viral dynamics. Gestational stage emerged as a key factor influencing

776 infection outcomes: specifically, infection initiated during early pregnancy (7.5–8.5 dpc)
777 and analyzed at 9.5–10.5 dpc identified a window of increased susceptibility to fetal
778 exposure, associated with the detection of infectious viral loads in fetal tissue. In contrast,
779 infection occurring during mid-gestation (13.5–14.5 dpc) and analyzed at 15.5–16.5 dpc
780 was associated with restricted detection of infectious virus in fetal tissues, despite
781 evidence of viral antigen persistence and sustained viral presence in maternal and
782 placental compartments. The detection of infectious viral particles in reproductive tissues
783 supports the biological plausibility of alternative transmission routes, although their
784 epidemiological relevance remains uncertain. These findings provide a comprehensive
785 experimental framework to advance the understanding of MAYV pathogenesis, systemic
786 dissemination and maternal–fetal involvement and potential non-vector transmission.

787 # References

788 1. Organization PAH. Epidemiological Alert: Mayaro Fever (1 May 2019) 2019.
789 [Available from: https://iris.paho.org/items/4fb69ec2-020d-4b35-8333-872092a2f88b.
790 2. Blohm G, Elbadry MA, Mavian C, Stephenson C, Loeb J, White S, et al. Mayaro
791 as a Caribbean traveler: Evidence for multiple introductions and transmission of the virus
792 into Haiti. Int J Infect Dis. 2019;87:151-3.
793 3. Ganjian N, Riviere-Cinnamond A. Mayaro virus in Latin America and the
794 Caribbean. Rev Panam Salud Publica. 2020;44:e14.
795 4. Valencia-Marin BS, Gandica ID, Aguirre-Obando OA. The Mayaro virus and its
796 potential epidemiological consequences in Colombia: an exploratory biomathematics
797 analysis. Parasit Vectors. 2020;13(1):508.

798 5. Brustolin M, Bartholomeeusen K, Rezende T, Arien KK, Muller R. Mayaro virus,
799 a potential threat for Europe: vector competence of autochthonous vector species. Parasit
800 Vectors. 2024;17(1):200.
801 6. Celone M, Beeman S, Han BA, Potter AM, Pecor DB, Okech B, et al.
802 Understanding transmission risk and predicting environmental suitability for Mayaro
803 Virus in Central and South America. PLoS Negl Trop Dis. 2024;18(1):e0011859.
804 7. Garcia-Romero C, Carrillo Bilbao GA, Navarro JC, Martin-Solano S, Saegerman
805 C. Arboviruses in Mammals in the Neotropics: A Systematic Review to Strengthen
806 Epidemiological Monitoring Strategies and Conservation Medicine. Viruses. 2023;15(2).
807 8. Andreolla AP, Borges AA, Bordignon J, Duarte Dos Santos CN. Mayaro Virus:
808 The State-of-the-Art for Antiviral Drug Development. Viruses. 2022;14(8).
809 9. Diagne CT, Bengue M, Choumet V, Hamel R, Pompon J, Misse D. Mayaro Virus
810 Pathogenesis and Transmission Mechanisms. Pathogens. 2020;9(9).
811 10. Marinho MDS, Ferreira GM, Grosche VR, Nicolau-Junior N, Campos TL, Santos
812 IA, et al. Evolutionary Profile of Mayaro Virus in the Americas: An Update into Genome
813 Variability. Viruses. 2024;16(5).
814 11. Cereghino C, Roesch F, Carrau L, Hardy A, Ribeiro-Filho HV, Henrion-Lacritick
815 A, et al. The E2 glycoprotein holds key residues for Mayaro virus adaptation to the urban
816 Aedes aegypti mosquito. PLoS pathogens. 2023;19(4):e1010491.
817 12. Mendonca DC, Reis EVS, Arias NEC, Valencia HJ, Bonjardim CA. A study of
818 the MAYV replication cycle: Correlation between the kinetics of viral multiplication and
819 viral morphogenesis. Virus Res. 2023;323:199002.
820 13. Ribeiro-Filho HV, Coimbra LD, Cassago A, Rocha RPF, Guerra J, de Felicio R,
821 et al. Cryo-EM structure of the mature and infective Mayaro virus at 4.4 A resolution
822 reveals features of arthritogenic alphaviruses. Nature communications. 2021;12(1):3038.

14. Krokovsky L, Lins CRB, Guedes DRD, Wallau GD, Ayres CFJ, Paiva MHS. Dynamic of Mayaro Virus Transmission in Mosquitoes and a Mice Model. Viruses-Basel. 2023;15(3).

15. Pereira TN, Virginio F, Souza JI, Moreira LA. Emergent Arboviruses: A Review About Mayaro virus and Oropouche orthobunyavirus. Frontiers in Tropical Diseases. 2021;Volume 2 - 2021.

16. de Thoisy B, Gardon J, Salas RA, Morvan J, Kazanji M. Mayaro virus in wild mammals, French Guiana (vol 9, pg 1326, 2003). Emerg Infect Dis. 2003;9(12):1659-.

17. Silva-Ramos CR, Mejorano-Fonseca JA, Hidalgo M, Rodríguez-Morales AJ, Faccini-Martinez AA. Clinical, Epidemiological and Laboratory Features of Mayaro Virus Infection: a Systematic Review. Curr Trop Med Rep. 2023;10(4):309-19.

18. de Curcio JS, Salem-Izacc SM, Neto LMP, Nunes EB, Anunciacao CE, Silveira-Lacerda ED. Detection of Mayaro virus in mosquitoes circulating in Goiania-Goias-Brazil. Microbes and Infection. 2022;24(4).

19. Brasil P, Pereira JP, Moreira ME, Nogueira RMR, Damasceno L, Wakimoto M, et al. Zika Virus Infection in Pregnant Women in Rio de Janeiro. New Engl J Med. 2016;375(24):2321-34.

20. Vermillion MS, Lei J, Shabi Y, Baxter VK, Crilly NP, McLane M, et al. Intrauterine Zika virus infection of pregnant immunocompetent mice models transplacental transmission and adverse perinatal outcomes. Nature communications. 2017;8.

21. Ramful D, Carbonnier M, Pasquet M, Bouhmani B, Ghazouani J, Noormahomed T, et al. Mother-to-child transmission of Chikungunya virus infection. Pediatr Infect Dis J. 2007;26(9):811-5.

847 22. Gerardin P, Barau G, Michault A, Bintner M, Randrianaivo H, Choker G, et al.
848 Multidisciplinary prospective study of mother-to-child chikungunya virus infections on
849 the island of La Reunion. PLoS Med. 2008;5(3):e60.
850 23. Pancetti FG, Honorio NA, Urbinatti PR, Lima-Camara TN. Twenty-eight years
851 of Aedes albopictus in Brazil: a rationale to maintain active entomological and
852 epidemiological surveillance. Rev Soc Bras Med Trop. 2015;48(1):87-9.
853 24. Mota MTO, Costa VV, Sugimoto MA, Guimaraes GF, Queiroz-Junior CM,
854 Moreira TP, et al. In-depth characterization of a novel live-attenuated Mayaro virus
855 vaccine candidate using an immunocompetent mouse model of Mayaro disease. Scientific
856 reports. 2020;10(1):5306.
857 25. Santos FM, Dias RS, de Oliveira MD, Costa I, Fernandes LS, Pessoa CR, et al.
858 Animal model of arthritis and myositis induced by the Mayaro virus. PLoS Negl Trop
859 Dis. 2019;13(5):e0007375.
860 26. Caetano CCD, Camini FC, Almeida LT, Ferraz AC, da Silva TF, Lima RLS, et
861 al. Mayaro Virus Induction of Oxidative Stress is Associated With Liver Pathology in a
862 Non-Lethal Mouse Model. Scientific reports. 2019;9.
863 27. de Carvalho AC, Dias CSB, Coimbra LD, Rocha RPF, Borin A, Fontoura MA, et
864 al. Characterization of Systemic Disease Development and Paw Inflammation in a
865 Susceptible Mouse Model of Mayaro Virus Infection and Validation Using X-ray
866 Synchrotron Microtomography. International Journal of Molecular Sciences. 2023;24(5).
867 28. Rosa RB, de Castro EF, Santos DD, da Silva MV, Pena LJ. Mouse Models of
868 Mayaro Virus. Viruses-Basel. 2023;15(9).
869 29. Weger-Lucarelli J, Carrau L, Levi LI, Rezelj V, Vallet T, Blanc H, et al. Host
870 nutritional status affects alphavirus virulence, transmission and evolution. PLoS
871 pathogens. 2019;15(11):e1008089.

872 30. Powers AM, Aguilar PV, Chandler LJ, Brault AC, Meakins TA, Watts D, et al.
873 Genetic relationships among Mayaro and Una viruses suggest distinct patterns of
874 transmission. Am J Trop Med Hyg. 2006;75(3):461-9.
875 31. Chuong C, Bates TA, Weger-Lucarelli J. Infectious cDNA clones of two strains
876 of Mayaro virus for studies on viral pathogenesis and vaccine development. Virology.
877 2019;535:227-31.
878 32. Acosta-Ampudia Y, Monsalve DM, Rodriguez Y, Pacheco Y, Anaya JM,
879 Ramirez-Santana C. Mayaro: an emerging viral threat? Emerg Microbes Infect.
880 2018;7(1):163.
881 33. Figueiredo CM, Neris RLD, Gavino-Leopoldino D, da Silva MOL, Almeida JS,
882 dos-Santos JS, et al. Mayaro Virus Replication Restriction and Induction of Muscular
883 Inflammation in Mice Are Dependent on Age, Type-I Interferon Response and Adaptive
884 Immunity. Front Microbiol. 2019;10.
885 34. Whitten WK. Modification of the oestrous cycle of the mouse by external stimuli
886 associated with the male; changes in the oestrous cycle determined by vaginal smears.
887 The Journal of endocrinology. 1958;17(3):307-13.
888 35. Roszkowski M, Mansuy IM. High Efficiency RNA Extraction From Sperm Cells
889 Using Guanidinium Thiocyanate Supplemented With Tris(2-Carboxyethyl)Phosphine.
890 Front Cell Dev Biol. 2021;9:648274.
891 36. Zhou Y, Zhou B, Pache L, Chang M, Khodabakhshi AH, Tanaseichuk O, et al.
892 Metascape provides a biologist-oriented resource for the analysis of systems-level
893 datasets. Nature communications. 2019;10(1):1523.
894 37. Llamas-González YY, Campos D, Pascale JM, Arbiza J, González-Santamaría J.
895 A Functional Ubiquitin-Proteasome System is Required for Efficient Replication of New
896 World Mayaro and Una Alphaviruses. Viruses-Basel. 2019;11(4).

897 38. Valdés-Torres P, Campos D, Bhakta M, Galán-Jurado PE, Durant-Archibold AA,
898 González-Santamaría J. Honokiol and Alpha-Mangostin Inhibit Mayaro Virus
899 Replication through Different Mechanisms. Molecules. 2022;27(21).
900 39. Atkins GJ, Carter J, Sheahan BJ. Effect of Alphavirus Infection on Mouse
901 Embryos. Infection and immunity. 1982;38(3):1285-90.
902 40. Taylor M, Rayner JO. Immune Response to Chikungunya Virus: Sex as a
903 Biological Variable and Implications for Natural Delivery via the Mosquito. Viruses-
904 Basel. 2023;15(9).
905 41. Hoen B, Schaub B, Funk AL, Ardillon V, Boullard M, Cabié A, et al. Pregnancy
906 Outcomes after ZIKV Infection in French Territories in the Americas. New Engl J Med.
907 2018;378(11):985-94.
908 42. Hcini N, Lambert V, Picone O, Carod JF, Carles G, Pomar L, et al. Arboviruses
909 and pregnancy: are the threats visible or hidden? Trop Dis Travel Med. 2024;10(1).
910 43. Megli CJ, Coyne CB. Infections at the maternal-fetal interface: an overview of
911 pathogenesis and defence. Nature Reviews Microbiology. 2022;20(2):67-82.
912 44. Wu YT, Su KZ, Zhang Y, Liang LC, Wang F, Chen SY, et al. A spatiotemporal
913 transcriptomic atlas of mouse placentation. Cell Discov. 2024;10(1).
914 45. DIRECTIVE 2010/63/EU OF THE EUROPEAN PARLIAMENT AND OF THE
915 COUNCIL on the protection of animals used for scientific purposes. Official Journal of
916 the European Union, L 276, 20 October 2010.
917 46. Avoiding, Minimizing and Alleviating Distress. Recognition and Alleviation of
918 Distress in Laboratory Animals. The National Academies Collection: Reports funded by
919 National Institutes of Health. Washington (DC)2008.

47. Rosa RB, Castro EF, Santos DO, Dantas WM, Tanaka CA, Mendes RPG, et al. A comprehensive murine clinical model for development of countermeasures and studying Mayaro virus infection. PLoS Negl Trop Dis. 2025;19(7):e0013333.

Acknowledgments

We thank José González Santamaría from the Department of Genomics and Proteomics Research, Gorgas Memorial Institute for Health Studies, Panama, for providing the primary antibody used in this study.

Author contributions

Conceptualization: APA, GM and MC. Methodology: APA, PP, JLP, MPG, BV, JMV, GM and MC. Investigation: APA, PP, JLP, MPG, GG, BV, JMV, GM and MC. Visualization: APA, PP, JLP, MPG, GG, BV, JMV, GM and MC. Statistical Analysis: APA. Supervision: GM and MC. Writing—original draft: APA, PP, JLP, GG, JMV, GM and MC. Writing—review & editing: APA, PP, JLP, MPG, GG, JH, AF, BV, JMV, GM and MC. Project administration: GM and MC. Funding acquisition: GM and MC. All authors agreed to submit the manuscript and have read and approved its final version. Authors take full responsibility for its content.

Funding

Institut Pasteur de Montevideo and FOCEM (COF 03/11), G4 program Institut Pasteur de Montevideo.

Competing interests

941 The authors declare no competing interests.

942 Data availability statement

943 All data supporting the findings of this study are available in accordance with
944 PLOS data sharing policies within the manuscript and its Supporting Information files.

945 Supporting information

946 **S1 Fig. Additional hematological and renal parameters during acute MAYV**
947 **infection.** Monocytes (A), eosinophils (B), basophils (C), red blood cells (RBC) (D), hemoglobin (E),
948 hematocrit (F), creatinine (G) and blood urea nitrogen (BUN) (H) were measured at 24 and 48 hours post-
949 infection (hpi) and in mock controls. Each dot represents an individual animal; horizontal lines indicate
950 median values. Black symbols denote pre-infection measurements and open symbols denote post-infection
951 measurements. For hematological analyses, n = 12 mice per time point; mock controls, n = 4. For
952 biochemical analyses, n = 6 mice at 24 hpi and n = 4 mice at 48 hpi; mock controls, n = 4. Sample sizes
953 varied depending on the parameter analyzed. Statistical analyses were performed using mixed-effects
954 models (REML) for repeated measures. Differences were considered statistically significant at $p < 0.05$ (*),
955 $p < 0.01$ (**) and $p < 0.001$ (***).

956

957 **S1 Table. Differentially expressed genes in placental tissues from MAYV-infected**
958 **mice at early (7.5–8.5 DPC) and mid (13.5–14.5 DPC) gestation compared with**
959 **stage-matched controls.**

960

961 **S2 Fig. Additional biochemical and metabolic parameters during acute MAYV**
962 **infection.** Total protein (A), albumin (B), globulin (C), total bilirubin (D), gamma-glutamyl transferase
963 (GGT) (E), blood urea nitrogen/creatinine ratio (BUN/CRE) (F), glucose (G) and body weight (H) were
964 measured at 24 and 48 hours post-infection (hpi) and in mock controls. Each dot represents an individual

965 animal; horizontal lines indicate median values. Black symbols denote pre-infection measurements and
966 open symbols denote post-infection measurements. For hematological analyses, n = 12 mice per time point;
967 mock controls, n = 4. For biochemical analyses, n = 6 mice at 24 hpi and n = 4 mice at 48 hpi; mock
968 controls, n = 4. Sample sizes varied depending on the parameter analyzed. Statistical analyses were
969 performed using mixed-effects models (REML) for repeated measures. Differences were considered
970 statistically significant at $p < 0.05$ (*), $p < 0.01$ (**) and $p < 0.001$ (***).

971

972 **S3 Fig. Red blood cell and platelet indices during acute MAYV infection.**
973 Mean corpuscular volume (MCV) (A), mean corpuscular hemoglobin (MCH) (B), mean corpuscular
974 hemoglobin concentration (MCHC) (C), red cell distribution width–coefficient of variation (RDW-CV)
975 (D), red cell distribution width–standard deviation (RDW-SD) (E), mean platelet volume (MPV) (F),
976 platelet distribution width (PDW) (G) and procalcitonin (H) were measured at 24 and 48 hours post-
977 infection (hpi) and in mock controls. Each dot represents an individual animal; horizontal lines indicate
978 median values. Black symbols denote pre-infection measurements and open symbols denote post-infection
979 measurements. For hematological analyses, n = 12 mice per time point; mock controls, n = 4. For
980 biochemical analyses, n = 6 mice at 24 hpi and n = 4 mice at 48 hpi; mock controls, n = 4. Sample sizes
981 varied depending on the parameter analyzed. Statistical analyses were performed using mixed-effects
982 models (REML) for repeated measures. Differences were considered statistically significant at $p < 0.05$ (*),
983 $p < 0.01$ (**) and $p < 0.001$ (***).

984

985 **S4 Fig. Exploratory analysis of infection-associated hematological changes across**
986 **gestational stages.** (A) Neutrophil percentage, (B) lymphocyte percentage, (C) total white blood cell
987 (WBC) count, (D) red blood cell (RBC) count, (E) platelet (PLT) count and (F) procalcitonin (PCT) levels
988 were measured at 48 hpi in females infected at early (7.5–8.5 dpc) and mid-gestation (13.5–14.5 dpc),
989 compared with their respective mock controls. Data are presented as individual values with median lines.
990 Infected groups: early gestation (n = 6) and mid-gestation (n = 7); mock controls (n = 2 per stage). Statistical
991 analyses were performed using two-way ANOVA with Sidak's multiple comparisons test. Data distribution
992 was assessed to verify test assumptions. Given the limited sample size of mock controls, statistical

comparisons involving these groups should be interpreted with caution. Differences were considered statistically significant at $p < 0.05$ (*), $p < 0.01$ (**) and $p < 0.001$ (***).